Catena 211 (2022) 105965

Contents lists available at ScienceDirect

Catena

journal homepage: www.elsevier.com/locate/catena

Genesis and stability of textural pedofeatures along a soil transect in the siliceous Iberian Chain (NE Spain)

David Badía-Villas [a,*], Rosa M. Poch [b], Luis A. Longares [c], Alfonso Yuste [d], Blanca Bauluz [d]

[a] Agrarian and Environmental Sciences Department, IUCA, University of Zaragoza, Technological College of Huesca, Spain
[b] Department of Environment and Soil Sciences, University of Lleida Spain
[c] Geography Department, IUCA, University of Zaragoza, Spain
[d] Earth Sciences Department, IUCA, University of Zaragoza, Spain

ARTICLE INFO

Keywords:
Clay coatings
Clay infillings
Deformed pedofeatures
Micromorphology
Classification
Polygenetic soils

ABSTRACT

Textural features are widespread in many soils, provide pedogenetic evidence, and are fundamental in soil classification systems. The presence of these features and their conservation over time require certain processes and soil forming factors. This study investigates the genesis of textural pedofeatures, especially clay coatings, and the stressful conditions that can eventually lead to their disappearance. To achieve this goal, four profiles with clay-enriched horizons have been studied (macro- and micromorphology, physical, chemical and mineralogical properties and classification) along a transect in the siliceous Iberian Chain (NE-Spain).

The profiles, which have unmistakable illuvial accumulations in various horizons (Bhs, Bt, Btk), are classified (ST/WRB) as: a Spodosol/Podzol in the headslope, two Alfisol/Luvisols in the backslope and an Alfisol/Calcisol in the footslope. For the latter soil, the apparently strong difference in their classification to the first hierarchical level is due to the weight that the WRB places on the presence of an argic recarbonated horizon on a calcic horizon.

Clay illuviation was identified in all the soils, with coatings and infillings of microlaminated clay. These clayey pedofeatures are mostly mechanically fragmented or deformed, which is micromorphologically evidenced by an undulating, wavy extinction that does not run completely parallel to the surfaces they cover. Different destructive processes are identified along the soil transect; so, cryoturbation is the dominant process in the Podzol located at the highest elevation (Moncayo Massif). Instead, the clay coatings in the Btk horizon of the footslope (Calcisol) are covered and deformed by the growth of secondary calcite. The textural pedofeatures in this soil, which is very clayey, can also undergo argilloturbation processes, like in the backslope soils (Luvisols). In conclusion, several ongoing stress processes, that sometimes require different environmental conditions (polygenetic), affect most textural pedofeatures and lead to their progressive alteration and disappearance.

1. Introduction

The increase of certain amounts of clay in a given horizon serves as a diagnostic criterion in the main soil classification systems, even at high hierarchical levels by means of different diagnostic horizons, such as agric, argillic, glossic, kandic and natric in USDA soil taxonomy, ST (Soil Survey Staff, 2014) or argic, natric and nitic horizons in World Reference System for Soil Resources (IUSS Working group WRB, 2015). Clay-enriched horizons fulfilling the requirements of argillic diagnostic horizon (from Latin *argilla*, clay) are fundamental in ST at various taxonomic levels in 10 of their 12 orders. Thus, it is essential at the order level (in Alfisols and Ultisols), as well as at the suborder (Aridisols), great group (in Aridisols, Gelisols, Mollisols, Oxisols, Vertisols), and subgroup levels (Andisols, Aridisols, Inceptisols, Mollisols, Oxisols, Spodosols). In Mediterranean regions of the world, argillic horizons are common, especially representative of Alfisols. This order of ST occupies approximately 6 million hectares in Spain—12.3% of the country—, with Ultisols occupying less than 0.2% (Gómez-Miguel and Badía-Villas, 2016). Soils with argillic horizons have a specific set of morphological, physical, chemical and mineralogical properties in addition to the clay increase, which is at least partially related to their illuviation. In the WRB this clay illuviation is not required to define the argic diagnostic horizon (IUSS Working group WRB, 2015). In the WRB, five reference soil groups (RSGs) contain the argic horizon as diagnostic: Acrisols,

* Corresponding author.
E-mail address: badia@unizar.es (D. Badía-Villas).

https://doi.org/10.1016/j.catena.2021.105965
Received 10 October 2021; Received in revised form 27 November 2021; Accepted 19 December 2021
Available online 27 December 2021

Alisols, Luvisols, Lixisols, and Retisols (formerly Albeluvisols), which correspond essentially with suborders of the Alfisols and Ultisols in ST (Soil Survey Staff, 2014). These five RSGs occupy approximately 16.7% of the world surface, with more than 2,500 million hectares (IUSS Working group WRB, 2015). Moreover, the presence of argic horizons (by means of the qualifiers Acric, Lixic, Alic or Luvic) is common in very different environmental conditions, and therefore, they are also present in other RSGs, either as principals (in Calcisols, Cryosols, Chernozems, Durisols, Ferralsols, Gypsisols, Kastanozems, Nitisols, Phaeozems, Planosols, Stagnosols and Umbrisols) or supplementary qualifiers (in Anthrosols and Gleysols). Even in Calcisols and Gypsisols, an argic horizon permeated throughout with secondary carbonate or secondary gypsum can be found above the calcic or gypsic horizon, respectively, reflecting conditions of increasing aridity (Silva et al., 2019).

In ST, the argillic horizon is "normally a subsurface horizon with a significantly higher percentage of phyllosilicate clay than the overlying soil material. This horizon shows evidence of clay illuviation" (Soil Survey Staff, 2014). Although not all the vertical increase in clay content from the surface horizons to the argillic one may be due to the illuviation of clay into the argillic horizon, it may be responsible for at least some of the increase. In the WRB, an argic horizon is a "subsurface horizon with distinctly higher clay content than the overlying horizon"; this textural differentiation may be the result of translocation, in situ formation or other processes (IUSS Working Group WRB, 2015). In the WRB, soils with the argic horizon developed by the accumulation of clay by physical movement or illuviation are assigned with the Cutanic qualifier. The argillic and illuvial argic horizons show thin sections with clay coatings, oriented clay bridges or oriented clay bodies as textural pedofeatures, as a consequence of clay movement. This movement usually takes place in three steps:

1. Clay from surface horizons is dispersed and thereby mobilized (peptization of clay), which in calcareous non-sodic soils requires a previous leaching of calcium
2. It is mobilized downwards in suspension, for which a sufficient amount of water is required.
3. The transported clay is deposited by simple filtration through fine pores and/or by reaggregation to accumulate (flocculation of clay) as clay coatings (where clay particles are oriented parallel to the walls).

These steps take place throughout alternating rainy/cold seasons, when eluviation of clays occurs after dispersion, with drier periods, when clay flocculates and accumulates in the subsurface horizon (argic/argillic). These conditions are typical in Mediterranean regions of the world (Bridges et al., 1998; Gómez-Miguel and Badía-Villas, 2016) although soils with clay-enriched horizons can be found in areas in almost any soil temperature and moisture regime. Very arid environments are where this process is less likely occur and, in fact, when they are found, they are attributed to paleo-processes, according to the review carried out by Bockheim and Hartemink (2013). Also, base-rich soils are not conducive to the genesis of clay skins, and such pedofeatures are considered the result of a past argilluviation process (De Arruda et al., 2021). In the South Pre-Pyrenean area, some clay-illuviated Bt horizons have been identified without being correlated to the age of the geoform in which they develop (Poch et al., 2019); this can be explained because the soil parent material are pedosediments, where processes act fast. Moreover, other pedogenic processes can be overimposed on textural processes, such as calcification, freezing and thawing or bioturbation. The identification of these processes, by means of thin sections, can be used as proxies of environmental changes (Kühn et al., 2018; Silva et al., 2019).

The aim of this work is to provide a model of soil evolution in the Iberian Range (NE-Spain), where clay illuviation overlaps with other seemingly incompatible processes of soil formation. To achieve this goal, the physical, chemical, mineralogical, and morphological soil properties of selected profiles were studied along a transect, from a headslope to a footslope geoform. Particular emphasis is placed on the soil's micromorphological description, mainly on the textural pedofeatures, and its relationship with environmental factors that may affect its state of conservation.

2. Materials and methods

2.1. Area of study

A soil transect, oriented northwest to southeast over a total distance of 80 km, was studied in the southeastern sector of the siliceous Iberian Range, NE Spain (Fig. 1). Along this transect, four profiles were selected within the montane stage, at elevations of between 1590 and 770 m above sea level, to provide reliable data for the interpretation of the region's soil-forming processes. This altitudinal gradient offers a gradient in the factors of soil formation (Table 1). Specifically, the mean annual precipitation ranges from 1112 mm/yr in the headslope to 438 mm/yr in the footslope, with a bimodal distribution of rainfall throughout the year (spring and autumn) and a summer drought, which is especially pronounced at lower levels (Serrano-Notivoli et al., 2017). The mean annual temperatures range from 6,3 °C at the highest altitude, with common snow events every winter, to 11.7 °C at the footslope (Serrano-Notivoli et al., 2019). Soil temperature/moisture regimes (Soil Survey Staff, 2014) are frigid/udic at the headslope and mesic/xeric at the backslope and footslope. In relation to the soil parent material, the headslope profile (Moncayo massif) is developed on a stony colluvium, originated by lobes of solifluction in mantle (Pellicer and Echevarría, 2004), dominated by angular quartz-rich and micaceous sandstones (Triassic Tierga Formation), placed near San Gaudioso hermitage (Badía et al., 2016). The Aniñón and Sestrica profiles, on the backslope, are located specifically in one of the fault uplifted blocks or horsts raised in the Sierra de la Virgen, in a northwest-southeast orientation relief, also on quartzites and siliceous sandstones of Paleozoic age. The Orcajo profile (footslope) is placed on a Pleistocene glacis composed of pedosediments—eroded soil from the backslope that is rich in quartzites and red clays from the Sierra de la Santa Cruz. All the profiles are located on slopes but with steep slopes (30%) at the top and very smooth slopes (3%) at the foot of the transect. More details on other formation factors are provided in Table 1.

2.2. Soil sampling and analysis.

The pedons were described according to FAO guidelines (FAO, 2006) and classified according to the WRB (IUSS Working group WRB, 2015) and ST (Soil Survey Staff, 2014). For each mineral horizon, we reported their morphological characteristics, including color, structure, consistency and accumulations for each pedon. Soil samples were air-dried and sieved (mesh size 2 mm) to determine the percentage of gravel (>2 mm) and fine earth (<2 mm). Laboratory analyses were performed on this last fraction. Particle size distribution (USDA classes) was determined by the discontinuous sedimentation method after removal of organic content with H_2O_2 (30%) and clay dispersal with 5% Na-hexametaphosphate (Gee and Bauder, 1986), without removal of carbonates. The Sand:(Sand + Coarse silt) ratio was calculated for each soil sample to distinguish colluviation (lithologic discontinuities) from illuviation processes in each profile. This was possible given that the distribution of the coarse soil fraction (sand and coarse silt) does not vary with soil depth and does not evolve through pedogenesis, unless the fraction is composed of highly weathered minerals such as carbonate (Esfandiarpour-Borujeni et al., 2018).

Soil pH was determined from potentiometric measurements of a 1:2.5 (w/v) suspension of soil and water (pH-H_2O) and with 1 N KCl (pH-KCl) (McLean, 1982). The cation exchange capacity (CEC) and exchangeable base cations were determined by NH_4^+ retention after leaching with a neutral solution of 1 N NH_4OAc (Rhoades, 1982). Clay CEC (CEC_{clay}) was calculated by using the following equation:

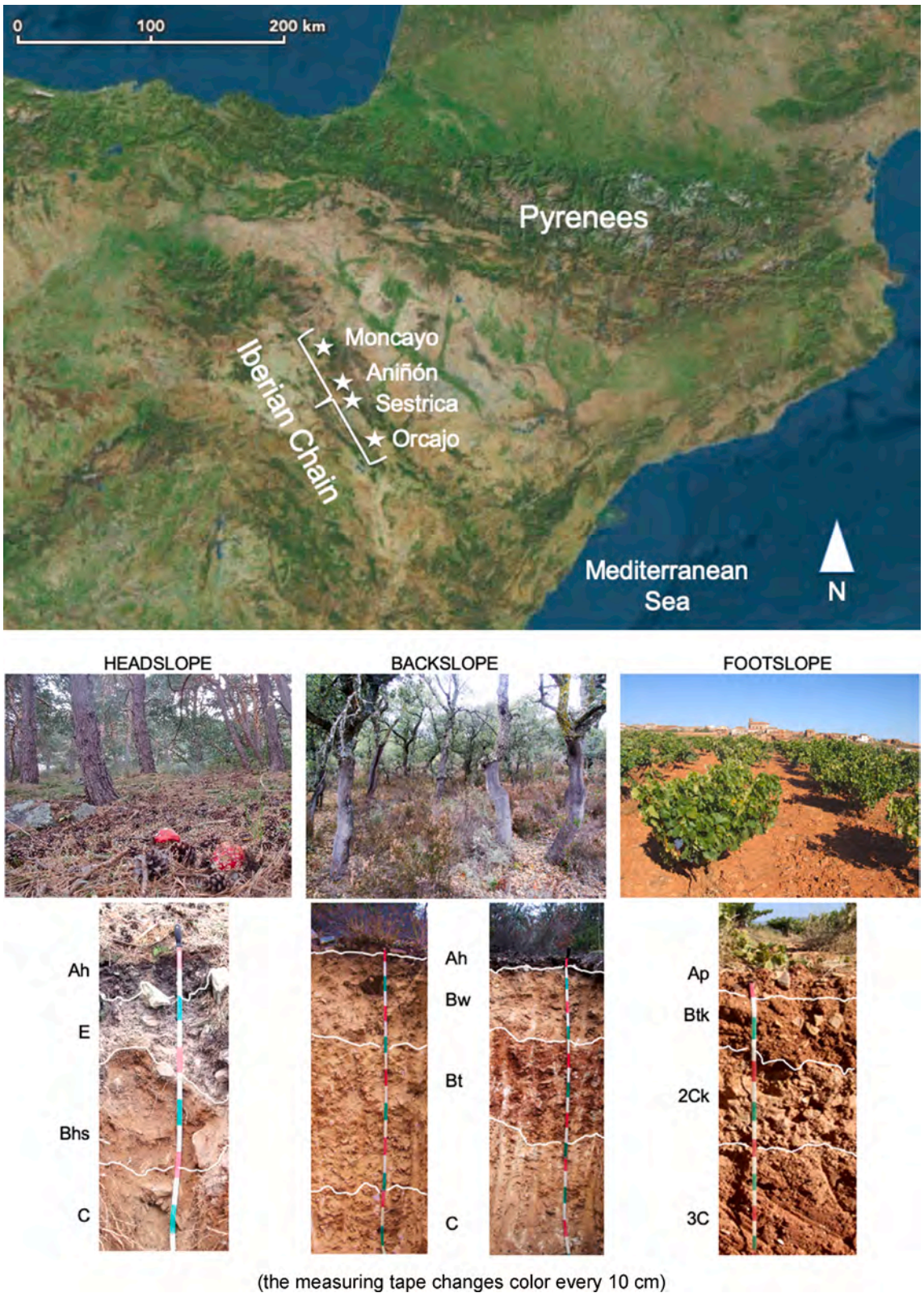

Fig. 1. Location of soil profiles studied along a transect in the Iberian Chain (NE-Spain).

$$CEC = (CEC_{clay} \times clay) + (CEC_{OM} \times OM),$$

considering that the CEC of the organic matter (CEC_{OM}) is 200 cmol/kg OM

Al and Fe were extracted with ammonium oxalate (Al_{ox} and Fe_{ox}) in the headslope profile (Blakemore, 1985) and analyzed by inductively coupled plasma optical emission spectrometry (ICP-OES). Total carbonates were measured volumetrically (Nelson, 1982). Organic carbon was determined by the wet oxidation method (Nelson and Sommers, 1982), and organic matter was calculated using the van Bemmelen factor. Total N was determined by the Kjeldahl method (Bremner and

Table 1
Factors of formation of studied pedons.

Location	Geomorphology Slope, Aspect	UTM location (30 T) X Y	Altitude (m)	Parent material	Climate MAP & MAT	Vegetation	Soil Sequum
Moncayo	Headslope 30%, NE	0,598,480 4,626,904	1590	Angular quartzite sandstone colluvium	1,112 mm 6.3 °C frigid, udic*	*Pinus sylvestris* *Ilex aquifolium* *Vaccinum myrtillus* *Erica vagans* *Erica arborea*	O-Ah-E-Bhs-C
Aniñón	Backslope 10%, W	0,606,990 4,595,253	977	Angular quartzites colluvium	486 mm 10.6 °C mesic, xeric *	*Quercus suber* *Quercus ballota* *Calluna vulgaris* *Cistus laurifolius*	O-Ah-BA-Bw-Bt1-Bt2-C
Sestrica	Backslope 10%, NE	06,136,541 4,495,755	802	Quartzites (Cambrian)	465 mm 11.4 °C mesic, xeric *	*Quercus suber* *Calluna vulgaris* *Cistus laurifolius* *Halimium umbellatum*	O-Ah-Bw1-Bw2-Bt-Ct-R
Orcajo	Footslope 3%, NE	0,627,005 4,551,793	770	Colluvium of red clays with subangular quartzites	438 mm 11.7 °C mesic, xeric *	*Vitis vinifera* fields	Ap-Btk-Ck-2C

Abbreviations: MAP, Mean annual precipitation & MAT, Mean annual temperature.
* Soil temperature & moisture regime (USDA).

Mulvaney, 1982).

For the study of soil micromorphology, undisturbed oriented soil samples were extracted, placed in containers, and transported to the laboratory to prepare thin sections, maintaining its original structure. Peds were air-dried, impregnated under vacuum with epoxy resin, and mounted on glass slides (5 x13 cm) to be ground at 30 μm, following Benyarku and Stoops (2005). Thin sections were examined using a petrographic microscope under both plane- and cross-polarized light (PPL and XPL), being photographed and interpreted following the guidelines of Stoops (2021).

The Pearson correlation coefficient (R) was calculated to evaluate the degree of linear association among variables; the correlation coefficients presented in the text are statistically significant at the $P < 0.01$ level, unless otherwise noted.

2.3. Mineralogical characterization

The mineralogy of both, fine earth fraction and clay fraction was determined by X-ray diffraction (XRD), using a Philips 1710 diffractometer, with 40 kV, 30 mA current, CuKα radiation, an automatic divergence slit and a graphite monochromator. The clay fraction was separated by centrifugation and was analyzed on air-dried and ethylene glycol-treated (at 60 °C for 48 h) oriented aggregates. The oriented aggregates were prepared by suspending 250 mg of sample in 6 mL of deionized water. A 0.5 mL volume of that suspension was pipetted onto a glass slide (27 × 47 mm), and air-dried. Diffraction patterns were scanned from 3 to 60 °2θ (random powder mounts) and from 3 to 30 °2θ (oriented aggregates). In both cases, a goniometer velocity of 0.1 °2θ/s and an integration time of 0.45 s were used. The XRD patterns were performed, recorded and stored using the XPowderX software (Martín, 2017).

Semi-quantitative estimates of mineral phases were carried out using the normalized Reference Intensity Ratio (RIR) method (Jenkins and Snyder, 1996) to compare among the studied samples; the RIR values of Schultz (1964) and Biscaye (1965), in accordance to Hillier (2003), were used for the estimation of mineral concentrations. Since the semi-quantification of chlorite + kaolinite is obtained as a whole from the overlapping 002 and 001 reflections of chlorite and kaolinite, respectively, the estimation of the existence of both minerals has been made by analyzing the presence of a double reflection at about 25 °2θ, corresponding to the 004 and 002 reflections of chlorite and kaolinite, respectively.

3. Results and discussion

3.1. Macromorphological, physical and chemical properties

The studied profiles have an intense horizonation, with a O-Ah-E-Bhs-C sequence in the headslope (Moncayo), O-Ah-Bw-Bt-C in both profiles of the backslope (Aniñon and Sestrica) and Ap-Btk-2Ck-3C in the footslope profile (Orcajo). Most horizons have a moderate reddish hue (Chromic), weak or moderate blocky structure, and slightly hard or hard dry consistency (Table 2). All the soils of the studied transect show different accumulations in different genetic horizons: organic matter, iron, aluminum and even clay (Bhs), clay (Bt) and clay and secondary carbonates (Btk). Clay-enriched horizons on backslopes (Aniñon and Sestrica) are deep and thick, more than in the rest of the slope forms. This may be the result of the higher stability offered by the backslopes compared to actively eroding shoulders and accumulative footslopes receiving new sediments (as it is compiled by Bockheim and Hartemink, 2013). A high quartzite fragment content (>40% v/v) have been found in most profiles (Skeletic qualifier). Both the circulation of water and even the translocation of suspended silicate clays are more readily caused by this “rock effect” (Bruckert and Bekkary, 1992) or kinematic porosity (Nasri et al., 2015). Fauna activity (such as insect excrements, ant galleries and worm burrows), roots and mycelia, have been identified, especially in the topsoil horizons (Table 2).

The soil in the headslope (Moncayo) has a sandy-loam texture; both soils in the backslope (Sestrica and Aniñón) range from sandy loam to sandy clay loam with soil depth, and the one in the footslope (Orcajo) has a clay textural class (Table 3).

The sand:(sand + coarse silt) ratio does not vary significantly in the headslope and backslope profiles. However, in the footslope profile (Orcajo) this ratio rises and falls abruptly with soil depth, just as stoniness does. This confirms the presence of two lithological discontinuities, at 35 and 80 cm depth (Table 3), between the Btk horizon and the 2Ck horizon, as well as between the 2Ck horizon and the 3C horizon (Amphiraptic qualifier).

Along the profile sequence, the soils showed a gradient in soil reaction: from very acidic in the headslope (Moncayo) to acidic in the backslope soils (Aniñón and Sestrica) to basic in the footslope (Orcajo). The pH range between 5 and 6.5 is favorable for clay illuviation, conditions that currently only exist on the backslope profiles. At pH values below 5 (as in Moncayo), clay flocculates due to the high Al^{3+} availability (Spaargaren and Deckers, 2005). On the other hand, at pH values

Table 2
Macromorphological characteristics of the soils described.

Location (RSG)	Horizon	Thickness (cm)	Color (Dry)	Color (Wet)	Stones (%, v/v)	Structure	Compaction	Biological activity	Roots abundance	Accumulations
Moncayo	Ah	0–18	7.5YR 3/1	10YR 2/1	50	s, G	SO	Common	Many	
(PZ)	E	18–30/50	7.5YR 6/2	7.5YR 4/2	50	no	SHA	Common	Common	
	Bhs	30/50–85	7.5YR 4/4	7.5YR 3/3	50	m, Sbk	SHA	Common	Common	OM, Fe/Al, clay
	C	85–110	10YR 6/3	10YR 4/3	60	no	SHA	None	Few	
Aniñón	Ah	0–5	7,5YR 5/2	7,5YR 3/2	20	w, Sbk	SO	Common	Common	
(LV)	BA	5–30	7,5YR 7/3	7,5YR 5/4	30	w, Sbk	SHA	Few	Common	
	Bw	30–70	7.5YR 7/3	7.5YR 5/4	40	w, Sbk	SHA	Few	Very few	
	Bt/Bw	70–90	7.5YR 7/4	7.5YR 5/6	50	m, Abk	HA	Few	Very few	clay
	Bt1	90–120	7.5YR 6/6	5YR 5/6	60	w, Abk	HA	Few	Very few	clay
	Bt2	120–150	7.5YR 6/6	5YR 5/6	60	w, Abk	HA	None	Very few	clay
	C	150–200	7.5YR 6/6	5YR 5/6	80	no	HA	None	None	
Sestrica	Ah	0–5	7,5YR 4/2	7,5YR 3/2	50	m, Sbk	SO	Common	Common	
(LV)	Bw1	5–30	7.5YR 7/4	7.5YR 5/4	30	m, Sbk	SHA	Few	Common	
	Bw2	30–70	7.5YR 7/4	7.5YR 5/4	40	m, Sbk	SHA	Few	Very few	
	Bt	70–100	5YR 5/6	5YR 4/6	50	m, Abk	HA	Few	Very few	clay
	Ct	100–130	5YR 6/6	5YR 5/6	80	no	HA	None	Very few	
Orcajo	Ap	0–10	5YR 5/6	5YR 4/6	25	m, Abk	SHA	Few	Few	
(CL)	Btk	10–35	5YR 5/6	5YR 4/6	30	m, Abk	HA	Few	Few	clay, CO_3Ca^1
	2Ck	35–80	5YR 6/6	2.5YR 4/6	60	no	HA	None	Very few	CO_3Ca^2
	3C	80–150	2.5YR 5/6	2.5YR 3/6	20	no	HA	None	None	CO_3Ca^3

Abbreviations: Grade of structure; no, no structure; w, weak; m, moderate; s, strong. Form: G, granular; Abk, Angular blocky, Sbk, Sub-angular blocky. Dry consistence: LO, loose or non-coherent; SO, soft; SHA, slightly hard; HA, hard. Accumulations: OM, Organic Matter, Fe/Al, Iron and aluminium (OxA), clay, illuviated clay; CO_3Ca, secondary carbonates: [1] pendents, fine and few, and coatings in ped faces, few; [2] pendents, medium and many, matrix slightly cemented; [3] coatings in ped faces, few

Table 3
Physical properties of the soils studied.

Location (RSG)	Horizon	Thickness (cm)	Stones (%, w/w)	Sand (%, w/w)	Silt (%, w/w)	Clay (%, w/w)	Texture class (USDA)	S/S + Cs ratio
Moncayo	Ah	0–18	75.0	59.8	36.8	13.4	Sandy Loam	0.80
(PZ)	E	18–30/50	60.4	62.1	31.0	6.9	Sandy Loam	0.80
	Bhs	30/50–85	59.9	56.7	30.6	12.7	Sandy Loam	0.80
	C	85–110	85.1	61.3	31.4	7.0	Sandy Loam	0.78
Aniñón	Ah	0–5	31.9	75.5	16.2	8.3	Sandy Loam	0.98
(LV)	BA	5–30	38.8	59.5	36.4	4.1	Sandy Loam	0.73
	Bw	30–70	59.4	53.9	40.2	5.9	Sandy Loam	0.70
	Bt/Bw	70–90	52.3	41.7	39.5	18.8	Loam	0.65
	Bt1	90–120	43.1	43.2	33.8	23.0	Loam	0.69
	Bt2	120–150	45.5	47.7	32.4	19.9	Loam	0.70
	C	150–200	60.2	54.5	28.4	17.1	Sandy Loam	0.79
Sestrica	Ah	0–5	38.5	75.5	18.8	5.7	Sandy Loam	0.88
(LV)	Bw1	5–30	23.0	71.2	24.0	4.8	Sandy Loam	0.87
	Bw2	30–70	31.1	66.7	25.7	7.6	Sandy Loam	0.85
	Bt	70–100	43.3	45.2	23.9	30.9	Sandy clay Loam	0.81
	Ct	100–130	57.7	50.0	20.6	29.6	Sandy clay Loam	0.86
Orcajo	Ap	0–10	32.3	31.5	23.6	44.9	Clay	1.04
(CL)	Btk	10–35	35.7	25.9	18.4	55.7	Clay	1.04
	2Ck	35–80	56.5	38.2	17.5	44.3	Clay	1.78
	3C	80–150	32.8	31.6	17.2	51.2	Clay	1.31

Abbreviations:
S/S + CS ratio: Sand/(Sand + Coarse silt) ratio; being Sand: 2000–50 μm and Coarse silt: 50–20 μm, particle size.

higher than 6.5 (as in Orcajo) and in the absence of Na^+, clay flocculates due to the high concentration of Ca^{2+} and Mg^{2+} in the solution, which act as cationic bridges between the negatively charged particles (Quénard et al., 2011; De Arruda, et al., 2021). The basic reaction in the footslope soil (Orcajo), with a maximum in the intermediate horizons (pH 8.5), is related to the calcium carbonate content (with a maximum of 23%, w/w, in the 2Ck horizon). In this profile, even the clay-enriched horizon is permeated throughout with secondary carbonates (Bkt), with calcium carbonate coatings both in the faces of the aggregates and undersides of gravels and stones (pendents), which are thicker in the underlying horizon (2Ck)—the depth with maximum pendent thickness or "bulge" (Badía-Villas et al., 2009).

Base saturation is significantly correlated with the pH-H_2O ($r = 0.94$; $p < 0.01$), so base saturation ranges from desaturated in the headslope soil (BS < 25%) to saturated (100%) in the footslope. Backslope soils are oligosaturated (20–50%) and mesosaturated (50–80%) in (Table 4).

In the set of soils, CEC is positively correlated with organic C content ($r = 0.81$; $p < 0.01$) and clay-size particle content ($r = 0.25$; $p > 0.05$), although in the latter case in a non-significant way. Organic C and noncarbonate clay content are the variables that commonly predict CEC (Seybold et al., 2005). CEC-clay values correspond to moderate-activity clays (10–40 cmol/kg clay), such as phyllosilicates 1:1 (kaolinite) and 2:1 (illite or chlorite), as will be confirmed in the next section.

In the headslope profile (Moncayo), the Bhs horizon has an amount of $(Al + 1/2Fe)_{ox}$ higher than 0,5% and > 2 times higher than the lowest value of all mineral horizons above it (spodic horizon). This is proof of iron and aluminum cheluviation, as well as organic matter, in addition to some clay accumulation. These processes indicate a high degree of weathering, directly associated with the high altitude (1590 m) at which this profile is located, and the resulting cold and wet climate (Serrano-Notivoli et al., 2017; 2019).

Table 4
Chemical properties of the analyzed soils.

Profile	Horizon	Depth	pH H_2O	pH KCl	$CaCO_3$ eq	Org C	C/N	Bases Sum	CEC $cmol_+$/kg	CECclay $cmol_+$/kg	BS	$(Al)_{ox}$	$(Fe)_{ox}$	$(Al + 1/2Fe)_{ox}$
		(cm)	(1:2.5)	(1:2.5)	(%)	(%)	(%)	($cmol_+$/kg)	of soil	of clay	(%)	(%)	(%)	(%)
Moncayo	Ah	0–18	4.1	3.1	0	10.0	22.1	6.16	43.0	128	14.3	0.121	0.143	0.192
(PZ)	E	18–30/50	4.0	2.9	0	1.2	11.5	2.18	8.9	69	24.4	0.057	0.065	0.089
	Bhs	30/50–85	5.2	4.0	0	3.1	18.5	3.44	27.1	129	12.7	0.988	0.802	1.389
	C	85–110	5.1	4.1	0	1.5	12.7	1.91	13.7	122	14.0	0.224	0.144	0.296
Aniñón	Ah	0–5	5.6	5.2	0	4.00	15.8	6.36	13.7	–	46.4	0.053	0.046	0.076
(LV)	BA	5–30	4.8	3.9	0	0.49	14.4	0.85	3.1	34	27.4	0.040	0.038	0.059
	Bw	30–70	5.2	4.1	0	0.33	13.1	1.28	3.5	40	36.6	0.041	0.046	0.064
	Bt/Bw	70–90	5.8	4.4	0	0.24	11.9	4.18	7.6	36	55.0	0.075	0.063	0.107
	Bt1	90–120	5.8	4.2	0	0.20	8.2	5.47	10.1	41	54.2	0.091	0.077	0.130
	Bt2	120–150	5.6	4.1	0	0.16	8.8	4.09	8.7	41	47.0	0.085	0.065	0.117
	C	150–200	5.4	4.0	0	0.09	4.7	3.10	8.0	45	38.8	0.084	0.072	0.120
Sestrica	Ah	0–5	6.4	6.3	0	3.71	13.2	8.60	11.4	68	75.4	0.025	0.040	0.045
(LV)	Bw1	5–30	5.2	4.0	0	0.28	17.5	1.59	3.9	81	40.8	0.041	0.056	0.068
	Bw2	30–70	5.3	3.9	0	0.28	13.3	1.98	4.4	58	45.0	0.048	0.059	0.078
	Bt	70–100	6.1	4.6	0	0.26	10.0	9.43	14.1	46	66.9	0.138	0.128	0.202
	Ct	100–130	6.2	4.5	0	0.20	10.5	9.30	13.5	45	68.9	0.112	0.151	0.169
Orcajo	Ap	0–10	8.2	7.5	7.3	2.19	10.1	19.7	19.7	44	100	nd	nd	nd
(CL)	Btk	10–35	8.5	7.7	4.2	0.77	9.8	19.1	19.1	34	100	nd	nd	nd
	2Ck	35–80	8.5	7.8	22.8	0.30	7.7	15.3	15.3	35	100	nd	nd	nd
	3C	80–150	7.9	7.1	8.0	0.12	7.4	12.5	12.5	24	100	nd	nd	nd

Abbreviations: Bases Sum: Exchangeable Ca, Mg, K and Na (by 1 M NH_4OAc pH7); CEC: Cation Exchange capacity (by 1 M NH_4OAc pH7); BS. Bases saturation: (Bases sum/CEC)*100; Al_{ox}, Fe_{ox}: Active or amorphous Al, Fe compounds extracted by an acid ammonium oxalate solution; nd, not determined.
CEC_{clay} based in the expression CEC = (CEC_{clay} × clay) + (CEC_{OM} × MO) (with a CEC_{OM} of 200 cmol/kg OM).

3.2. Mineralogical characterization

The mineralogical composition of the fine fraction of soil profiles was dominated by quartz (35–87%) and phyllosilicates (13–29%), with presence (<5%) of (K-, Ca/Na-) feldspars and hematite (Fe_2O_3), which despite the small amount has a great soil reddening capacity (Torrent et al., 1983). Calcite is only present in the footslope profile (Orcajo), with the minimum found in the Btk horizon (5%) and a maximum in 2Ck (21%). There was also a good correlation with the equivalent calcium carbonate amount ($r = 0.98$; $p < 0.01$). Clay illuviation is usually inhibited in calcareous soil by a high Ca^{2+} and Mg^{2+} availability, but it is sufficient to decarbonate the upper part of the profile, at some point in its genesis, to mobilize the clay (Poch et al., 2013).

The quartz:phyllosilicates ratio decreases from 4:1 or 5:1 in the headslope and backslope profiles to 1:1 in footslope profiles. Moreover, the evolution of both main components (quartz and phyllosilicates) with soil depth is usually related to the process of clay illuviation, so that the phyllosilicates tend to reach their maximum in Bt-horizons (Table 5). The quartz content correlates with sand ($r = 0.81$; $p < 0.01$) and, to a lesser extent, with silt content ($r = 0.50$; $p < 0.05$), while the phyllosilicate amount correlates with clay-size particle content ($r = 0.94$; $p < 0.01$).

Table 5
Semi-quantitative mineralogical composition (relative abundance, %) of the fine earth fraction (≤2 mm), determined via X-ray diffraction, of the studied soil profiles.

Location (RSG)	Genetic Horizon	Depth (cm)	Quartz	Phyllo-silicates	Q/Ph-ratio	K-feldspars	Ca or Na-feldspars*	Hematites	Calcite
Moncayo	Ah	0–18	73	24	3.0	<5	<5	–	–
(PZ)	E	18–30/50	80	18	4.4	<5	<5	–	–
	Bhs	30/50–85	73	23	3.2	<5	<5	<5	–
	C	85–110	78	18	4.3	<5	<5	<5	–
Aniñón	Ah	0–5	82	16	5.1	<5	–	–	–
(LV)	BA	5–30	84	13	6.5	<5	<5	–	–
	Bw	30–70/90	83	13	6.4	<5	<5	–	–
	Bt1	70/90–120	71	25	2.8	<5	<5	–	–
	Bt2	120–150	74	23	3.2	<5	<5	–	–
	C	150–200	82	16	5.1	<5	<5	–	–
Sestrica	Ah	0–5	87	13	6.7	–	–	–	–
(LV)	Bw1	5–30	85	12	7.1	<5	<5	–	–
	Bw2	30–70	85	13	6.5	<5	<5	–	–
	Bt	70–100	68	29	2.3	<5	<5	–	–
	Ct	100–130	71	26	2.7	<5	<5	–	–
Orcajo	Ap	0–10	50	37	1.4	<5	<5	–	10
(CL)	Btk	10–35	53	38	1.4	<5	<5	<5	5
	2Ck	35–80	35	42	0.8	<5	<5	–	21
	3C	80–150	54	35	1.5	<5	<5	–	8

Values lower than 5 % indicates "presence".
-, not detected.
Q/Ph: Quartz: Phyllosilicates ratio.
* Ca or Na feldspars: Plagioclase.

On the other hand, the clay fraction consisted primarily of illite (44–71%), kaolinite + chlorite (8–41%) and quartz (8–29%). Illite is inherited from parent material. Along the soil transect, quartz decreases from headslope (Moncayo) to footslope (Orcajo), opposite to kaolinite and chlorite, which increase. Additionally, small amounts of smectite are found in the bottom horizons (Bt and C) of backslope and footslope profiles (Table 6); smectites are readily broken down into fine clays and translocated through the soil (Bockheim and Hartemink, 2013). Smectite, a high-activity clay (80–150 cmol/kg clay), is formed by weathering of micas in clay-enriched horizons, where ponding conditions can be favorable for its formation (Chesworth, 2008). Permeability, which can be high in the topsoil due to coarse textures and the stoniness (Bruckert and Bekkary, 1992; Nasri et al., 2015), relatively decreases upon reaching B horizons, as is demonstrated by the presence of microscopic redoximorphic features such as dendritic aggregate nodules (of iron and manganese) within the peds.

3.3. Soil classification

According to the aforementioned soil properties, the surface horizons of the studied soils can only be classified as ochric in ST. In the profile located at highest altitude (Moncayo), the Ah horizon fulfills the criteria of umbric diagnostic horizon except for the thickness criteria (less than 20 cm in WRB and less than 25 cm in ST). Under these conditions, the WRB would admit the qualifier of someriumbric. In this same profile, the E horizon can be classified as albic horizon/ albic material (ST/WRB) and the Bhs as spodic diagnostic horizon. Consequently, it is classified as Spodosol/Podzol (ST/WRB) at the first hierarchical level (see full names in Table 7). Some clay coatings lining certain surfaces in the pores, most of them fragmented, have been found in the lower part of the spodic horizon (Bhs); being part of a spodic horizon, it could be classified as argic if it had shown more evidence of clay illuviation (IUSS Working Group WRB, 2015). The WRB admits the combination of an illuvial spodic horizon with and argic horizon, desaturated in bases (BS < 50%) and clays of a quality of CEC ≥ 24 cmolc kg^{-1} clay (ie. Alic Podzol). The presence of argillic or kandic horizons, within 200 cm of the mineral soil surface, below a spodic horizon (and not above) is predicted at the subgroup level in the order of Spodosols of ST (Soil Survey Staff, 2014) with the qualifiers Alfic (if the argillic or kandic horizon has a base saturation of over 35 % in some part), or Ultic, (with a base saturation lower than 35 %). A hypothesis of two subhorizons within the defined spodic (Bhs, 30–85 cm) (consisting of a thinner, upper Bhs overlying a Bt) could be further studied, which would validate the proposed soil forming mechanisms, and, therefore, the possible presence of Alic Podzols in the Iberian Chain.

Table 6
Semi-quantitative mineralogical composition (relative abundance, %) of the clay fraction (≤2 μm), determined via X-ray diffraction, in the studied soil profiles.

Location (RSG)	Genetic Horizon	Depth (cm)	Quartz	Illite	Mixed layer Kaolinite + Chlorite	Smectite
Moncayo (PZ)	Ah	0–18	19	66	16	–
	E	18–30/50	25	60	15	–
	Bhs	30/50–85	29	54	17	–
	C	85–110	27	59	14	–
Aniñón (LV)	Ah	0–5	27	64	9	–
	BA	5–30	24	55	21	–
	Bw	30–70/90	22	53	25	–
	Bt1	70/90–120	12	60	22	6
	Bt2	120–150	14	63	19	<5
	C	150–200	15	62	18	5
Sestrica (LV)	Ah	0–5	21	71	8	–
	Bw1	5–30	19	51	30	–
	Bw2	30–70	17	60	23	–
	Bt	70–100	8	57	32	<5
	Ct	100–130	11	57	27	5
Orcajo (CL)	Ap	0–10	10	63	27	–
	Btk	10–35	12	55	28	<5
	2Ck	35–80	8	48	41	<5
	3C	80–150	10	44	41	5

Values lower than 5 % indicates "presence".
-, not detected.

Table 7
Classification of soils studied along the Iberian Range (NE-Spain) transect.

Location	Geoform	Classification	
		WRB (2015)	SSS (2014)
Moncayo	Headslope	Skeletic Someriumbric Albic Podzol (Loamic)	Typic Haplorthod, loamy-skeletal, mixed, superactive, frigid
Aniñón	Backslope	Abruptic Chromic Skeletic Luvisol (Loamic, Epidystric, Ochric)	Ultic Haploxeralf, loamy-skeletal, illitic, active, mesic
Sestrica	Backslope	Abruptic Chromic Skeletic Luvisol (Loamic, Ochric)	Ultic Haploxeralf, loamy-skeletal, illitic, active, mesic
Orcajo	Footslope	Luvic Skeletic Calcisol (Pantoclayic, Aric, Ochric, Amphiraptic, Chromic)	Calcic Haploxeralf, clayey-skeletal, illitic, semiactive, mesic

At an intermediate altitude, in the backslope, both profiles (Aniñón and Sestrica) have very thin (0–5 cm) Ah horizons and thick Bt-horizons which fulfill the criteria for argillic/argic horizons. The intermediate B-horizons of both profiles have a marked eluvial character, at the definition limit of the "albic material", both in WRB and in ST, a concept for which there are certain differences between systems. These soils are classified as Alfisols/Luvisols, specifically as Ultic Haploxeralf/Abruptic Chromic Skeletic Luvisol (see full denomination in Table 7). The profile at the footslope (Orcajo) has a sequence of ochric-argillic-calcic (ST) or none-argic-calcic (WRB) diagnostic horizons. In this soil at lowest altitude, the argillic/argic horizon is permeated throughout with secondary carbonates, especially as coatings in the faces of the aggregates; for this reason, the soil belongs to the Calcisols WRB soil group. However, in ST it is classified within Alfisols order (Table 7). The different classification of the Orcajo soil under both taxonomies at the first hierarchical level is related to the distinction that WRB keys make regarding the re-carbonated argic on a calcic horizon, unlike ST. Thus, with the described horizon sequence (an argic/argillic horizon, permeated throughout with secondary carbonate, over a calcic horizon), the soil belongs to the WRB Calcisol group, which appears earlier in the key than the other RSGs with argic horizons not permeated with secondary carbonates (Retisols, Acrisols, Lixisols, Alisols and Luvisols). In contrast, the ST keys give priority to soils with argillic horizons (Alfisols) over soils with calcic ones (Inceptisols), without mentioning the re-carbonation or not of this argillic horizon. It could be interesting to contemplate this last criterion also in ST in order to harmonize both classification systems. In any case, the presence of a calcic horizon below the argic one classifies the soil as Calcic Haploxeralf. On the other hand, the addition of the "Humic" supplementary qualifier in the Calcisol RSG of the WRB is highly recommended, as it is already in many other groups. This is due to the fact that a weighted average of 1% soil organic carbon is easily reachable in the fine earth fraction up to a depth of 50 cm from the mineral soil surface (Badía-Villas and Del Moral, 2016). In Orcajo this value is 0.9%, that is, in the Ochric-Humic limit.

3.4. Pedofeatures: Micromorphology

In the Bhs horizon of the headslope (Podzol of Moncayo), the micromass is formed by clay and fine silt, amorphous organic matter, and iron oxides; its b-fabric is cristallitic-sericitic (micaceous). In the Bt

of both backslope Luvisols, the micromass is composed of sand, fine silt and iron oxides. Iron oxides are also present in the micromass of the Btk horizon of the footslope (Calcisol of Orcajo), although in this case with abundant clay as well as fine silt. The b-fabric is mosaic speckled in Bt horizons of the backslope profiles (Aniñón and Sestrica) and stipple speckled in the Btk horizon of the footslope (Orcajo). According to Stoops and Mees (2018), this b-fabric type reflects the presence of clay domains in the groundmass (Table 8).

Textural pedofeatures are common, mainly clay coatings in all the soil profiles studied (Bhs, Bt, Btk horizons). The most common types are microlaminated clay coatings and infillings, i.e., made of alternating thin (<30 μm) sheets of limpid and speckled clay. The limpid clay coatings are, in general, the result of illuvial clay (Stoops and Mees, 2018), with very fine clay (<0,02 μm) parallelly oriented to the wall of the soil pores. In the microlaminated clay, fine silt is also intercalated in the voids, both in Bhs of the Podzol and in Bt horizons of Luvisols (Fig. 2). Both clay coatings and infillings found in the studied profiles are deformed and fragmented. This may be a currently active process or an old process (Fedoroff and Courty, 2013; Stoops et al, 2020). In both cases, since these features are chemically stable, they may have been disturbed by different mechanical processes, ie: cryoturbation, recarbonation, argilloturbation and/or bioturbation. Specifically, the Podzol of the Moncayo is subjected to cryoturbation processes that explain the deformation of clay pedofeatures. At the altitude where it is located (1590 m), in a subalpine area, both cryonival geomorphological processes (Gómez et al. 2000) and periglacial processes (Pellicer and Echevarría, 2004) are common. These processes are active for almost 6 months per year and are especially intense in the winter season, since the minimum average temperature is −1.7 °C (Fick and Hijmans, 2017). Previous studies show how cryoturbation can be responsible for the destruction of clayey pedofeatures as well as the formation of silt cappings in Moncayo soils (Fibla et al., 2020). These silt cappings have been

Table 8
Main micromorphological properties of the groundmass of the studied profiles.

Headslope: PZ, Moncayo soil profile							
Horizon	**Microstructure**	**Porosity**	**Basal mass**	**Coarse elements**	**Micromass**	**Organic matter**	**Pedofeatures**
Bhs1	Granular with widely separated aggregates	50% composite packaging	c/f ratio: 1:2; c/f related dist: single space porphyric	Quartz, fragments of quartzite and micaceous sandstones	Clay, AOM, fine silt and Fe oxides. B-fabric is sericitic crystallitic (micaceous)	Fresh or phlobaphenized root sections	Silt cappings on top of coarse fragments (quartzitic sandstone) with voids underlying them
Bhs2	Apedial with vesicules and channels	30%	c/f ratio: 2:1; c/f related distribution: closed porphyric.	Quartz, fragments of quartzite and micaceous sandstones	Clay, AOM, fine silt and Fe oxides. B-fabric is sericitic crystallitic (micaceous)	Absent	Micro-laminated clay coatings and clay infillings occur in pores, most of them fragmented. Frequent orthic Fe-oxides nodules.

Backslope: LV, Aniñón soil profile								
Horizon		**Microstructure**	**Porosity**	**Basal mass**	**Coarse elements**	**Micromass**	**Organic matter**	**Pedofeatures**
Aniñón	Ah/BA	Crumbly in the surface, with aggregates close together, juxtaposed to widely separated angular blocks, abundant from the bottom	40%, composite packaging porus, channels and vughs	c/f ratio 1:2; c/f related distribution: close porphyric	Quartz and fragments of quartzite	Clay and fine silt, AOM. Undifferentiated b-fabric	Hyphae and sclerotia of fungi, plant remains partially decomposed by fauna	Excrement and pores of compound packing due to the formation of microaggregates by fauna
	Bt	Widely separated subangular blocks	20%, with fissures well accommodated, channels and vughs	c/f ratio: 4:1; c/f related distribution: random speckled	Quartz and fragments of quartzite	Sand, fine silt and iron oxides; b-fabric: speckled in mosaic	Absent	Iron oxide nodules. Clay hypocoatings. Microlaminated clay coatings. Clay infillings. Clay pedofeatures deformed and fragmented.
Backslope: LV, Sestrica soil profile								
Sestrica	Bt	Angular blocks, widely separated	30%, with fissures moderately accomodated, channels	c/f ratio: 4:1; c/f related distribution: random speckled	Quartz and fragments of quartzite	Sand, fine silt and iron oxides; b-fabric: speckled in mosaic	Plant remains partially decomposed by fauna	Iron oxide nodules. Clay hypocoatings. Microlaminated clay coatings. Clay infillings. Clay pedofeatures deformed and fragmented (the fragments mixed with the basal mass)

Footslope: CL. Orcajo soil profile								
Horizon		**Microstructure**	**Porosity**	**Basal mass**	**Coarse elements**	**Micromass**	**Organic matter**	**Pedofeatures**
Orcajo	Btk/2Ck	Subangular blocky, moderately separated; intrapedal channel	20%, with fissures, poorly accommodated (7%), channels and chambers (7%) and vesicles (6%)	c/f limit: 20μm; c/f ratio: 1/3; c/f related distribution: double to open porphyric.	very coarse sand of quartzites, subrounded; medium sand of quartz, equant angular; nodule fragments, rounded	clay, fine silt and iron oxides; b-fabric: stipple speckled.	None	1) frequent disorthic nodules of micrite, very coarse and coarse sand (up to 15% of the thin section); (2) interlaced infillings and coatings of needle-shaped calcite in channels; (3) clay coatings around pores, sometimes overlying previous coatings of needle-shaped calcite.

where; CP. composite packaging; c/f, coarse/fine; R.D., related distribution; AOM, amorph organic matter.

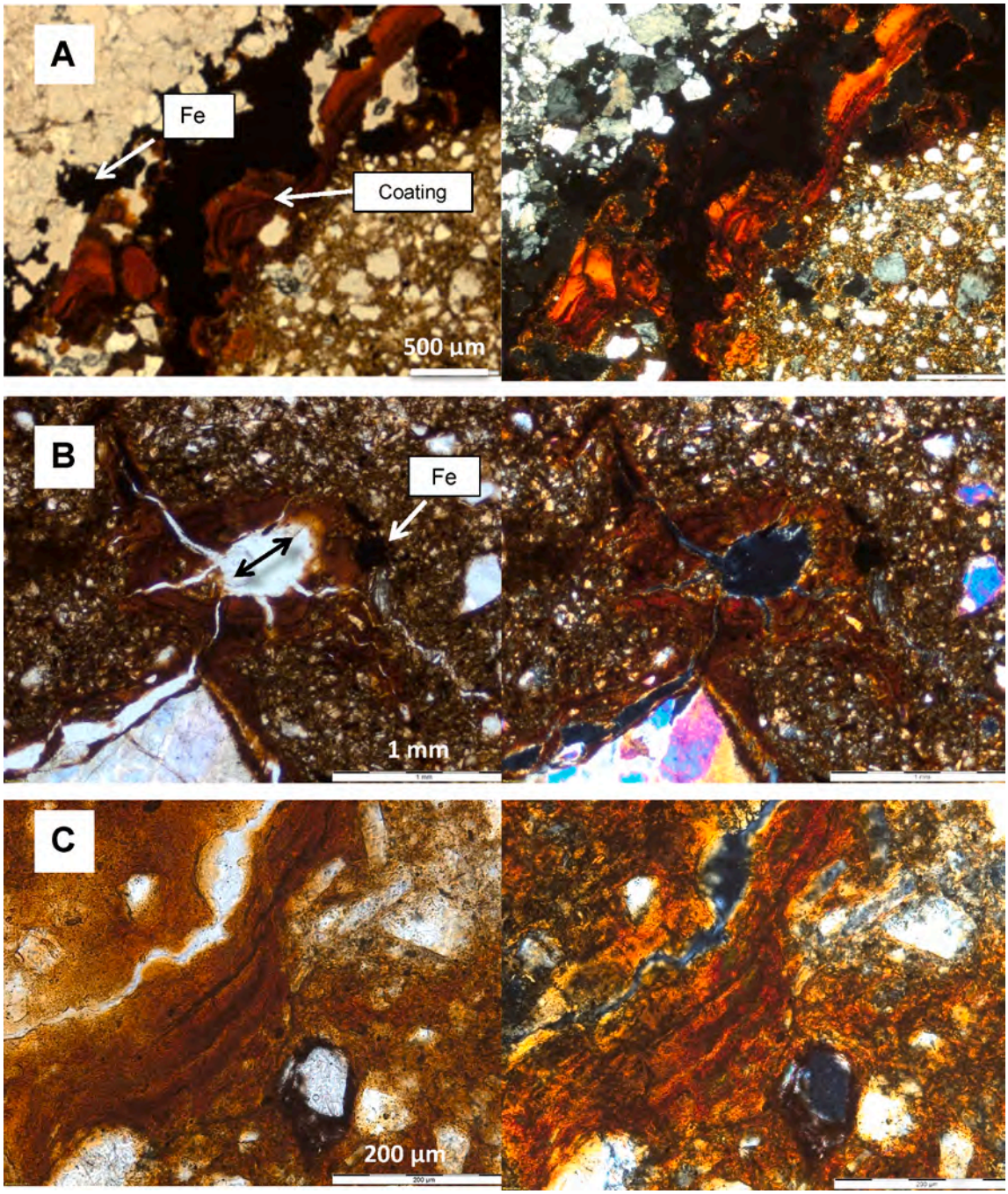

Fig. 2. *Clay coatings in the studied horizons.* Pictures in PPL, plane-polarized light (left) and XPL, cross-polarized light (right): **A:** Microlaminated clay coatings and nodules of Fe oxides (goethite) between a thick fragment of quartzite and the micromass in the Bhs horizon of the Podzol, Moncayo. Note that it is only found on one side, unrelated to the current pore space. The graphic scale is 500 µm. **B:** Microlaminated coating of clay in a vugh and in fissures of the Bt horizon of the Luvisol, Aniñón profile. Notice the cracking of the coating. The graphic scale is 1 mm. **C:** Thick microlaminated clay coating around a channel of the Bt horizon of the Luvisol, Sestrica profile. Some of the clay coatings were deformed; the alteration of the original microlamination would be a relict sign. The graphic scale is 200 µm.

observed both in the E horizon (18–30 cm) and at various depths of the Bhs horizon (30–85 cm). The development of silt cappings on coarse fragments and voids below them is linked to the formation and thawing of ice (Van Vliet-Lanoë and Fox 2018),

Additionally, in the Podzol, signs of intense fauna activity have been identified (excrements of collembola, diptera …) up to a depth of at least 60 cm; in the same soil, mixing of horizons by fauna has also been described (Fibla et al., 2020). In the remaining profiles, both empty and filled ant galleries and worm burrows, as well as roots and mycelia, have also been identified, which likely participate in the ground mass alteration. Fauna activity—burrowing and transporting material—is an important factor (bioturbation) capable of modifying the original textural pedofeatures. Nonetheless, the fauna-driven upward movement of fine particles can also encourage subsequent clay translocation (Phillips, 2007). In addition to bioturbation, certain shrinkage and swelling of expandable clays (argilloturbation) during common wetting and drying cycles (Khormali et al., 2003), can be responsible for the deformation or destruction of clayey pedofeatures in the Luvisols of the backslope. Smectite, even when present in low quantities (up to 6%), is heterogeneously distributed, so it may also have contributed to

deforming textural features. In any case, other clay types such as illites have swelling / shrinking properties, though to a lesser extent, that age the textural pedofeatures by deforming them and giving them a wavy appearance (Kuhn et al., 2018). In the footslope profile of CL-Orcajo, smectites have also been detected among the many clays (this profile has a clayey texture). In this case, however, another more important process plays a role in textural pedofeature deformation: profile recarbonation (Fig. 4A). The clayey pedofeatures are covered by needle-shaped calcite, that is, by acicular calcite crystals growing by precipitation in Ca^{2+}-saturated solutions (Fig. 4B). The recarbonation of the upper horizons of this profile can be related to colluviation and/or aeolian carbonate-containing contributions given the proximity of carbonate-rich Miocene sediments and young soils developed on them. Even though this calcite growth is interspersed with illuvial clay (Fig. 3C), this would provide evidence of the alternation of processes whose simultaneity would seem incompatible (Badía-Villas et al., 2013; Khormali et al., 2003). It has traditionally been considered that, except for sodic soils, clay translocation is promoted with a soil pH ranging from 5.5 to 6.5, when neither Ca^{2+} or Mg^{2+} nor Fe^{3+} or Al^{3+} (nor organic matter) act as binding agents (Quénard et al., 2011). For this reason, the clay illuviation in both the Podzol and the Calcisol could have happened under different conditions than the current ones: less acidic in first one and less basic in the second one.

The sequence of soil processes (clay illuviation-podzolization and clay illuviation-calcification) may be the result of:

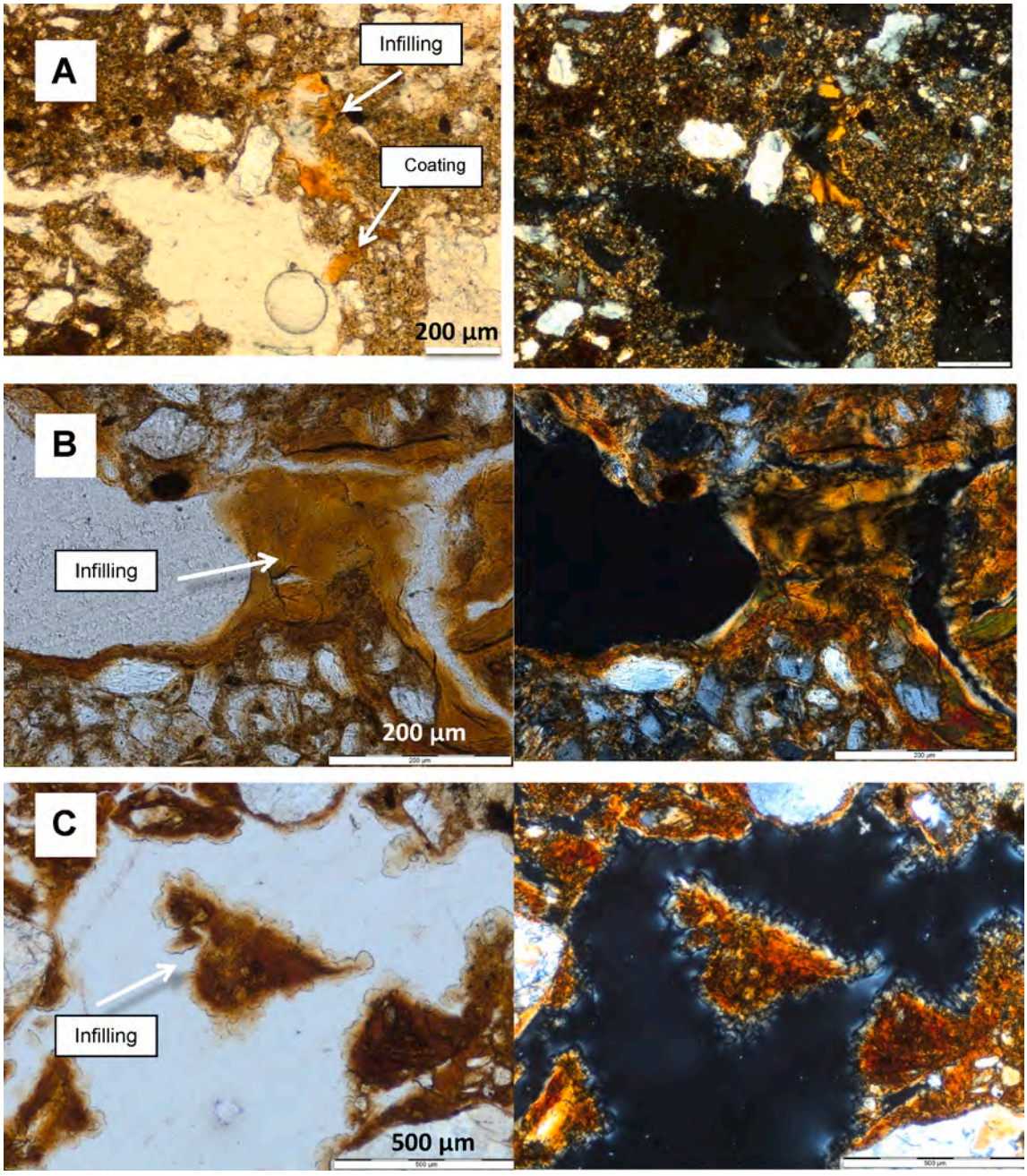

Fig. 3. *Infillings of clay in the studied horizons.* Pictures in PPL plane-polarized light (left) and XPL cross-polarized light (right). **A:** Microlaminated infilling and clay coating in pores of the Bhs2 horizon of the Podzol of the Moncayo. The graphic scale is 200 µm. **B:** Dense and incomplete clay infilling in a channel of the Bt horizon of the Luvisol of the Aniñón profile. The graphic scale is 200 µm. **C:** Loose and discontinuous clay infilling in a Bt horizon cavity of the Luvisol of the Sestrica profile. The graphic scale is 500 µm.

1) a threshold being overpassed, which would explain abrupt changes (Recio Espejo et al., 2008). In this sense, progressive acidification of the Moncayo Podzol can lead to a higher availability of Fe and Al oxides that stop clay illuviation and favors podzolization (Lundström et al., 2000). The substitution throughout the centuries of beech forests for pine forests at the Moncayo site may have helped soil acidification (D'Amico, et al., 2013). In any case, the presence of argillic or kandic horizons is predicted at the subgroup level in the order of Spodosols of ST (Soil Survey Staff, 2014).
2) periodic stages (Theory of biorhexistasy) rather than continuous ones (Bockheim et al., 2005), with episodes of soil formation (biostasy) followed by erosion or destruction (rhexistasy). For instance, in the Calcisol, the rubefaction-illuviation phase (pedogenetic phase) alternated with the pedosedimentary phase (Fedoroff et al. 2010; Świtoniak et al., 2016). Traditionally, decarbonation and desaturation are previous steps to argilluviation, so the basifying cations do not act as binding agents (Quénard et al. 2011). As it has been mentioned, if the upper part of the profile has been decarbonated at some point in its genesis, the clay can be eluviated (Poch et al., 2013). Also, the presence of hematite in the Btk horizon of the CL can indicate carbonate absence during formation, since calcite hinders weathering of Fe-bearing primary minerals (Torrent et al., 1983), as well as other environmental conditions (summer drought, well-drained conditions, low organic matter content…).

The existence of an argic-calcic sequence of the Luvic Calcisol of

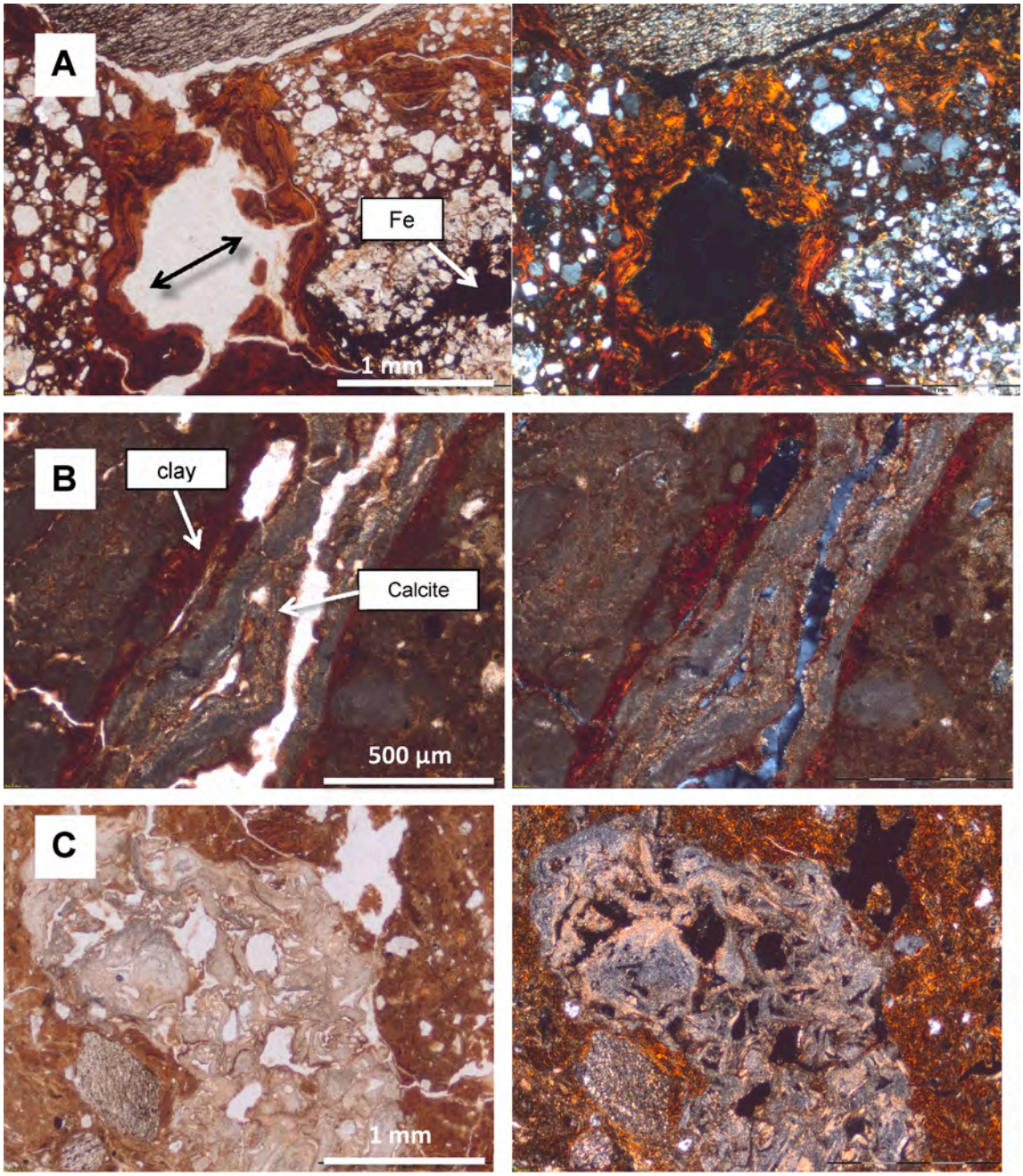

Fig. 4. *Microphotographs of the Btk horizon in the Calcisol of Orcajo soil.* Pictures in PPL, plane-polarized light (left) and XPL, cross-polarized light (right): **A:** Microlaminated clay and iron coatings and infillings between quartzites; clay coatings are deformed, indicating that it is an old process. The graphic scale is 1 mm. **B:** Clay coatings around pores interspersed with coatings of needle-shaped calcite, a feature indicating the overlap of processes. The graphic scale is 500 µm. **C:** Interlaced infillings and coatings of needle-shaped calcite in channels with some clay coatings overimposed on them. The graphic scale is 1 mm.

Orcajo, with the argic horizon having been recently recarbonated, is proof of environmental condition change during its genesis. The formation of this pedotype usually requires more humid conditions than the current ones (Khormali et al., 2003; Badía-Villas et al., 2013). In these current conditions, in which ET exceeded relative P (mm) and with a low plant cover, wind storms can transport and deposit calcite dust from nearby Miocene sediments and young soils rich in carbonates to the soil surface. In a soil chronosequence in the Reno River Valley (Italy), on Late Pleistocene to Holocene deposits, Eppes et al. (2008) found that the carbonate content in the profiles was not totally predictable by age due to the addition of colluvium and/or dust rich in carbonates to terrace surfaces older than ~ 12,000 years. Profiles with the argic over calcic sequence (i.e., pedotype Calcic Luvisol) require a certain development time and geomorphological stability, especially in dry climates; i.e., they are found in alluvial sequences of the mid-Medjerda floodplain (Northern Tunisia) on Late Pleistocene surfaces (Zielhofer et al., 2009).

The processes of illuviation and rubefaction on red Mediterranean soils must have occurred during interglacial periods, when the climate was humid (except for the dry and hot summers); and stopped in the more arid glacial intervals (discontinuous way). At the same time as the disruption of these processes, during glacial periods, aeolian inputs of calcite, as well as hydric erosion and colluvionation could occur. The deposition of calcium carbonate-rich aeolian dust would be followed by its redistribution in the soil profile via water (Fedoroff and Courty, 2013). However, when carbonate dissolution is found synchronously with illuviation (i.e., Fig. 4C), it can be interpreted that soil must have been formed in periods of environmental instability (continuous way) when soils were affected by various soil forming processes during short periods of time, such as from oxygen isotope stages 5d to 2 (Fedoroff and Courty, 2013). Additionally, the microlamination of clay coatings, found in the PZ and LVs, has been interpreted as a result of regular rain distribution, no excess water, and an interannual precipitation stability. This may have happened during interglacial periods of the whole Pleistocene in the Mediterranean basin (Fedoroff and Courty, 2013). Stoops et al (2020) also found many fragmented and/or deformed illuvial clay coatings in Belgian soils along a transect from the coast to the Ardennes, which was interpreted as a sign of an inactive illuviation process. Van Vliet-Lanoë and Langohr (1985) already considered that clay illuviation had its origin before the Last Glacial period.

Summarizing, the clay coatings and infillings found in all the studied soils rarely preserve the continuous orientation of clay what is attributed to different mechanical processes, such as: cryoturbation (PZ-Moncayo), recarbonation of the original Bt- horizon (CL-Orcajo profile), or argilloturbation (both in LVs and CL, with a high proportion of clays, mainly illtes and, some of them, smectites). In addition, the role of fauna on the clayey pedofeatures disappearance (bioturbation) should not be ruled out. Some of these processes have occurred simultaneously, yet others have occurred successively, in consecutive pedogenic processes (polygenetic soils), which is common in almost all natural soils (Stoops et al., 2020). The observed textural pedofeature instability might reflect a case of equifinality, whereby different processes or their combination leads to the same result (Phillips, 2007).

4. Conclusions

Subsoil horizons with an accumulation of clay have been found in all the studied profiles, with fewer or less illuviation features. In the highest profile (Moncayo), an illuvial spodic diagnostic horizon has been defined and soil is classified as Spodosol/Podzol. In the remaining soils, argic/argillic diagnostic horizons have been identified, and soils were classified as Alfisols/Luvisols, with the exception of the profile in the lowest altitude (Orcajo), where the argic is permeated throughout with secondary carbonate and classified as Calcisol by the WRB and as Alfisol by ST. Namely, the recarbonation of the argic/argillic horizon on a calcic horizon separates the same soil at the highest hierarchical level of both taxonomies.

Clay coatings and infillings of microlaminated clay can be found in the B-horizons of these soils, but they are mechanically fragmented or deformed. The deformation of these textural pedofeatures is shown by an undulating, wavy extinction that does not run completely parallel to the surfaces they cover or by the presence of textural pedofeatures that are not even related to the current porosity. The alteration of clayey pedofeatures is caused by different processes that overlap the previous clay illuviation. Therefore, at the highest altitude, in the Podzol of the headslope, clay coating deformation can be attributed to a current cryoturbation process. This is confirmed by other freeze–thaw features, such as silt cappings on the coarse elements with voids in their base. In argillic/argic horizons of both backslope Luvisols, the coatings and infillings may have been deformed by shrinking and swelling of clays (argilloturbation). Lastly, in the argillic/argic horizon of the footslope, clay coatings are covered by secondary calcite, which deforms and fossilizes the former clay illuviation process.

In conclusion, the textural pedofeatures observed in the soil transect studied in the Iberian Chain are subjected to conditions of mechanical stress that lead to their degradation and disappearance. This is due to the superposition of processes that sometimes require different environmental conditions (polygenetic soils), which is also indicative of the aging of the soils studied.

Declaration of Competing Interest

The authors declare that they have no known competing financial interests or personal relationships that could have appeared to influence the work reported in this paper.

Acknowledgments

Different projects of the Research Results Transfer Office of the University of Zaragoza (Ref. 2017/0535, ref. 2018/0416; ref. UZ2020-TEC-01) provided financial support for this research. The authors would also like to thank the three anonymous reviewers for their helpful suggestions that have improved this article.

References

Benyarku, C.A., Stoops, G., 2005. Guidelines for preparation of rock and soil thin sections and polished sections. In: Quaderns DMACS, 33 (ed. Universitat de Lleida). Lleida.
Badía, D., Ruiz, A., Girona, A., Martí, C., Casanova, J., Ibarra, P., Zufiaurre, R., 2016. The influence of elevation on soil properties and forest litter in the siliceous Moncayo Massif, SW Europe. J. Mt. Sci. 13 (12), 2155–2169.
Badía-Villas, D., Del Moral, F., 2016. Soils of Arid lands. In: The Soils of Spain (J.F. Gallardo Lancho. In: Coord.), Chapter, 4. Springer International Publishing, pp. 147–164.
Badía-Villas, D., Martí, C., Palacio, E., Sancho, C., Poch, R.M., 2009. Soil evolution over the Quaternary period in a semiarid climate (Segre river terraces, northeast Spain). Catena 77, 165–174.
Badía-Villas, D., Poch, R.M., García-González, M.T., 2013. Paleoclimatic implications of micromorphic features of a polygenetic soil in the Monegros Desert (NE-Spain). Spanish J. Soil Sci. 3 (2), 95–115.
Biscaye, P.E., 1965. Mineralogy and sedimentation of recent deep-sea clays in the Atlantic Ocean and adjacent seas and oceans. Geol. Soc. Am. Bull. 76, 803–831.
Blakemore, L.C., 1985. Acid oxalate-extractable iron, aluminium and silicon, ICOMAND. Circular Letter, 5. New Zealand Soil Bureau, Lower Hutt.
Bockheim, J.G., Gennadiyev, A.N., Hammer, R.D., Tandarich, J.P., 2005. Historical development of key concepts in pedology. Geoderma 124, 23–36.
Bockheim, J.G., Hartemink, A.E., 2013. Distribution and classification of soils with clay-enriched horizons in the USA. Geoderma 209–210, 153–160. https://doi.org/10.1016/j.geoderma.2013.06.009.
Bremner, J.M., Mulvaney, C.S., 1982. Nitrogen total. In: Page, A.L., Miller, R.H., Keeney, D.R. (Eds.), Methods of Soil Analysis. Part 2: Chemical and Microbiological Properties, 2nd edition. American Society of Agronomy, Madison, Wisconsin, pp. 595–624.
Bridges, E.M., Batjes, N.H., Nachtergaele, F.O., 1998. World Reference Base for Soil Resources: Atlas. Acco, Leuven.
Bruckert, S., Bekkary, M., 1992. Formation des horizons diagnostiques argiliques et de fragipan en fonction de la permeabilité des roches. Can. J. Soil Sci. 72, 69–88.
Cheswort, W. (ed.), 2008. Encyclopedia of Soil Science. Springer. 902 pp.
D'Amico, M.E., Freppaz, M., Filippa, G., Zanini, E., 2013. Vegetation influence on soil formation rate in a proglacial chronosequence (Lys Glacier, NW Italian Alps). Catena 113, 122–137.

De Arruda Silva, D.L., de Lima Camelo, D., de Araújo, C., Filho, J., Barros dos Santo, J.C., de Souza Junior, A.J., Souza, J.V., Metri Correa, M., 2021. Genesis of clay skins in tropical eutric soils: A case study from NE-Brazil. Catena 202, 105236.

Esfandiarpour-Borujeni, I., Mosleh, Z., Farpoor, M.H., 2018. Comparing the ability of Soil Taxonomy (2014) and WRB (2015= to distinguish lithological discontinuity and an abrupt textural change in major soils of Iran. Catena 165, 63–71.

FAO, 2006. Guidelines for soil description. 4th edition, 97 pp. Rome.

Fibla, N., Poch, R.M., Badía-Villas, D., 2020. Genesis of an atypical Podzol in the Iberian Range: micromorphological characterization. Spanish Journal of Soil Science 10 (3), 209–216. https://doi.org/10.3232/SJSS.2020.V10.N3.04.

Fick, S.E., Hijmans, R.J., 2017. WorldClim 2: new 1 km spatial resolution climate surfaces for global land areas. Int. J. Climatol. 37 (12), 4302–4315.

Eppes, M.C., Bierma, R., Vinson, D., Pazzaglia, F., 2008. A soil chronosequence study of the Reno valley, Italy: Insights into the relative role of climate versus anthropogenic forcing on hillslope processes during the mid-Holocene. Geoderma 147 (2008), 97–107.

Fedoroff, N., Courty, M.A., Guo, Z.T., 2010. Palaeosoils and relict soils. In: Stoops, G., Marcelino, V., Mees, F. (Eds.), Interpretation of micromorphological features of soils and regoliths. Elsevier, pp. 623–662.

Fedoroff, N., Courty, M.A., 2013. Revisiting the genesis of red Mediterranean soils. Turkish J Earth Sci. 22, 359–375.

Gee, G.W., Bauder, J.W., 1986. Particle-size analysis. In: Klute, A. (Ed.), Methods of soil analysis. Part 1: Physical and mineralogical methods, 2nd edition,. American Society of Agronomy, Madison, Wisconsin, USA, pp. 383–412.

Gómez, A., Martí-Bono, C., Salvador, F., 2000. Evolución reciente de los estudios de geomorfología glaciar y periglaciar en España (1980–2000): balance y perspectivas. Scripta Nova 77, Barcelona.

Gómez-Miguel, V.D., Badía-Villas, D., 2016. Soil distribution and classification. In: Gallardo, J.F. (Ed.), The Soils of Spain. Springer, Berlin, Germany. ISBN 978-3-319-20541-0.

Hillier, S., 2003. Quantitative analysis of clay and other minerals in sandstones by X-ray powder diffraction (XRPD). Int. Assoc. Sedimentologists. Spec. Publ. 34, 213–251.

IUSS Working Group WRB, 2015. World Reference Base for Soil Resources 2014: International soil classification system for naming soils and creating legends for soil maps. Updated 2015. World Soil Resources Reports, n° 106. FAO. Rome.

Jenkins, R., Snyder, R.L., 1996. Introduction to X-ray Powder Diffractometry. John Wiley & Sons, New York, p. 432.

Khormali, F., Abtahi, A., Mahmoodi, S., Stoops, G., 2003. Argillic horizon development in calcareous soils of arid and semiarid regions of southern Iran. Catena 53, 273–301.

Kühn, P. Aguilar, J., Miedema, R., Bronnikova, M., 2018. Textural pedofeatures and related horizons. Chapter 14: 377-423. In: Stoops, G., Marcelino, V., Mees, F. Interpretation of Micromorphological Features of Soils and Regoliths. Elsevier.

Lundström, U.S., Van Breemen, N., Bai, D., 2000. The podzolization process. A review. Geoderma 94, 91–107. https://doi.org/10.1016/S0016-7061(99)00036-1.

Martin, J.D., 2017. A software package for powder x-ray diffraction analysis. Qualitative, Quantitative and Microtexture, p. 121.

McLean, E.O., 1982. Soil pH and lime requirement. In: Page, A.L., Miller, R.H., Keeney, D.R. (Eds.), Methods of soil analysis. Part 2: Chemical and microbiological properties, 2nd edition,. American Society of Agronomy, Madison, Wisconsin. USA, pp. 199–224.

Nasri, B., Fouché, O., Torri, D., 2015. Coupling published pedotransfer functions for the estimation of bulk density and saturated hydraulic conductivity in stony soils. Catena 131, 99–108. https://doi.org/10.1016/j.catena.2015.03.018.

Nelson, R. E., 1982. Carbonate and gypsum. In: Page, A. L, Miller, R. H, and Keeney, D. R. eds., Methods of soil analysis. Part 2: Chemical and microbiological properties, 2nd ed. American Society of Agronomy, Madison, Wisconsin, USA,pp. 181–198.

Nelson, R.E., Sommers, L.E., 1982. Total carbon and organic matter. In: Page, A.L., Miller, R.H., Keeney, D.R. (Eds.), Methods of soil analysis. Part 2: Chemical and microbiological properties, 2nd edition. American Society of Agronomy, Madison, Wisconsin. USA, pp. 539–557.

Pellicer, F., Echeverría, M.T., 2004. El modelado glaciar y periglaciar en el macizo del Moncayo. En Peña, J.L., Longares, L.A. y Sánchez, M. (Eds.). Geografía Física de Aragón. Aspectos generales y temáticos. Universidad de Zaragoza e Institución Fernando El Católico. Zaragoza.

Phillips, J.D., 2007. Development of texture contrast soils by a combination of bioturbation and translocation. Catena 70, 92–104.

Poch, R.M., Simó, I., Boixadera, J., 2013. Benchmark soils on alluvial, fluvial and fluvio-glacial formation of the upper Segre valley. Spanish J. Soil Sci. 3, 78–94.

Poch, R.M., Balasch, J.C., Antúnez, M., Vadell, J., Forss, A., Boixadera, J., 2019. A distinct pedogenetic path under a Mediterranean climate: The case of soils on Areny sandstone formation (Tremp basin, NE Iberian Peninsula). In: Deák, J., Ampe, C., Mikkelsen, J.H. (Eds.), Soils as records of Past and Present. Raakvlak, Bruges, Belgium.

Quénard, L., Samouëlian, A., Laroche, B., Cornu, S., 2011. Lessivage as a major process of soil formation: A revisitation of existing data. Geoderma 167–168, 135–147.

Recio-Espejo, J.M., Faust, D., Nuñez-Granados, M.A., Zielhofer, C., 2008. Accumulation of secondary carbonate evidence by ascending capillary in Mediterranean argillic horizons (Cordoba, Andalusia, Spain). Soil Sci. 173, 350–358.

Rhoades, J.D., 1982. Cation exchange capacity. In: Page, A.L., Miller, R.H., Keeney, D.R. (Eds.), Methods of soil analysis. Part 2: Chemical and microbiological properties, 2nd edition,. American Society of Agronomy, Madison, Wisconsin. USA, pp. 149–158.

Schultz, L.G., 1964. Quantitative interpretation of mineralogical composition from X-ray and chemical data for the Pierre Shale. Professional Paper U.S, Geological Survey, p. 391C.

Serrano-Notivoli, R., Beguería, S., de Luis, M., 2017. SPREAD: a high-resolution daily gridded precipitation dataset for Spain – an extreme events frequency and intensity overview. Earth Syst. Sci. Data 9, 721–738. https://doi.org/10.5194/essd-9-721-2017.

Serrano-Notivoli, R., Beguería, S., de Luis, M., 2019. STEAD: a high-resolution daily gridded temperature dataset for Spain. Earth Syst. Sci. Data 11, 1171–1188. https://doi.org/10.5194/essd-11-1171-2019.

Seybold, C., Grossman, R., Reinsch, T., 2005. Predicting cation exchange capacity for soil survey using linear models. Soil Sci. Soc. Am. J. 69, 856–863.

Silva, M.L., Batezelli, A., Ladeira, F.S.B., 2019. Genesis and evolution of paleosols of the Marília Formation, Maastrichtian, of the Bauru Basin. Brazil. Catena 182, 104108.

Soil Survey Staff, 2014. Keys to Soil Taxonomy, 12th ed. USDA-Natural Resources Conservation Service, Washington, DC.

Spaargaren, O.C., Deckers, J.A., 2005. Factors of soil formation - Climate. 512-520 pp. In: Hillel, D (ed), Encyclopedia of Soils in the Environment, Elsevier.

Stoops, G., 2021. Guidelines for analysis and description of soil and regolith thin sections. 2nd ed. Soil Science Society of America, Madison, WI & John Wiley and sons.

Stoops, G., Mees, F., 2018. Groundmass composition and fabric. 73-125 pp. In: Stoops, G., Marcelino, V., Mees, F., (Eds) Interpretation of micromorphological features of soils and sediments. (2nd ed.). Elsevier, Amsterdam1000 pages.

Stoops, G., Langohr, R., Van Ranst, E., 2020. Micromorphology of soils and palaeosoils in Belgium. An inventory and meta-analysis. Catena 194, 104718. https://doi.org/10.1016/j.catena.2020.104718.

Świtoniak, M., Mroczek, P., Bednarek, R., 2016. Luvisols or Cambisols? Micromorphological study of soil truncation in young morainic landscapes — Case study: Brodnica and Chełmno Lake Districts (North Poland). Catena 137, 583–595.

Torrent, J., Schwertmann, V., Fechter, H., Alférez, F., 1983. Quantitative relationships between soil color and hematite content. Soil Sci. 136, 354–358.

Van Vliet-Lanoë, B., Langohr, R., 1985. Evidence of disturbance by frost of pore ferriargilans in silty soils of Belgium and Northern France. In: Bullock, P., Murphy, C. P. (Eds.) Soil Micromorphology. Volume 2. Soil Genesis. AB Academic Publishers, Berkhamsted, United Kingdom, pp. 511–518.

Van Vliet-Lanoë, B., Fox, C.A., 2018. Frost action. In: Stoops, G., Marcelino, V., Mees, F. (Eds.), Interpretation of micromorphological features of soils and regoliths, 2nd ed. Elsevier, Amsterdam, pp. 575–603.

Zielhofer, C., Recio-Espejo, J.M., Nuñez-Granados, M.A., Dominik, F., 2009. Durations of soil formation and soil development indices in a Holocene Mediterranean floodplain. Quat. Int. 209, 44–65.